Microchimica Acta
https://doi.org/10.1007/s00604-019-3256-5

ORIGINAL PAPER

A field effect transistor modified with reduced graphene oxide for immunodetection of Ebola virus

Xin Jin[1] · Hong Zhang[2] · Yu-Tao Li[1] · Meng-Meng Xiao[3] · Zhi-Ling Zhang[4] · Dai-Wen Pang[4] · Gary Wong[5,6] · Zhi-Yong Zhang[3] · Guo-Jun Zhang[1]

Received: 17 October 2018 / Accepted: 16 January 2019

Abstract

The authors describe a field effect transistor (FET) based immunoassay for the detection of inactivated ebola virus (EBOV). An equine antibody against the EBOV glycoprotein was immobilized on the surface of the FET that was previously modified with reduced graphene oxide (RGO). The antibody against EBOV was immobilized on the modified FET, and the response to EBOV was measured as a function of the shift of Dirac voltage. The method can detect the EBOV over the concentration range from 2.4×10^{-12} g·mL^{-1} to 1.2×10^{-7} g·mL^{-1} and with a limit of detection as low as 2.4 pg·mL^{-1}. The assay has satisfactory specificity and was applied to the quantitation of inactivated EBOV in spiked serum.

Keywords Ebola virus · Field effect transistor · Biosensor · Sensitive detection · Reduced graphene oxide · Immunoreaction

Introduction

Ebola virus (EBOV) is a highly pathogenic virus that invades most major organs and causes multisystem failure in humans. The mortality rate of diseases caused by EBOV infection can reach up to 90% [1–5]. Due to its high fatality rate and general, non-specific symptoms early in disease, rapid, selective, and sensitive detection has important implications in the field of early diagnosis.

The traditional diagnostic methods for Ebola virus disease (EVD) are the enzyme-linked immunosorbent assays [6, 7], immunofluorescence [8], and reverse-transcription polymerase chain reactions [9]. However, these methods are limited by the need for large sample amounts, complex pre-processing, time-consuming and low sensitivity. Additionally, these methods are only effective in detecting viral RNA or antigen in suspected patients with advanced disease and cannot directly detect EBOV at early stages [10–12]. An early diagnosis of

Xin Jin and Hong Zhang contributed equally to this work

Electronic supplementary material The online version of this article (https://doi.org/10.1007/s00604-019-3256-5) contains supplementary material, which is available to authorized users.

✉ Gary Wong
garyckwong@hotmail.com

✉ Zhi-Yong Zhang
zyzhang@pku.edu.cn

✉ Guo-Jun Zhang
zhanggj@hbtcm.edu.cn

[1] School of Laboratory Medicine, Hubei University of Chinese Medicine, 1 Huangjia Lake West Road, Wuhan 430065, People's Republic of China

[2] Teaching and Research Office of Forensic Medicine, Hubei University of Chinese Medicine, 1 Huangjia Lake West Road, Wuhan 430065, People's Republic of China

[3] Hunan Institute of Advanced Sensing and Information Technology, Xiangtan University, Xiangtan, Hunan 411105, People's Republic of China

[4] Key Laboratory of Analytical Chemistry for Biology and Medicine (Ministry of Education), College of Chemistry and Molecular Sciences, Wuhan University, Wuhan 430072, People's Republic of China

[5] Institut Pasteur of Shanghai, Chinese Academy of Sciences, Shanghai 200031, People's Republic of China

[6] Département de microbiologie-infectiologieetd'immunologie, Université Laval, Québec City, QC G1V 0A6, Canada

Published online: 07 March 2019

EBOV is essential to prevent the spread of the disease, enabling more effective treatments when there is an outbreak without warning. Although many sensitive assays, such as electroluminescence [13], luminescence resonance energy transfer strategy [14], and fluorescence counting strategies [15], etc., provide useful tools to directly measure EBOV with high sensitivity, the disadvantages to these methods are the cumbersome pre-treatment process. As an advanced method, biosensors based on reduced graphene oxide field effect transistors (RGO-FET) have obtained more and more attention in clinical diagnostics due to their attractive features. These purely electronic devices modified with specific receptor molecules are able to detect specific targets with capabilities of sensitive, selective sensing and rapid response. Better yet, FET biosensor is one of the most promising candidates in point-of-care (POC) diagnostics because it can be mass-produced using microfabrication technology [16–20]. Since EVD cases typically occur in rural areas, portability of testing is obviously necessary for the purposes of effective disease management. In such a case, POC testing devices for highly sensitive, smart and rapid detection of EBOV are highly desired. In our previous work, we have utilized the advantage of RGO-FET biosensors for detection of various analytes including nucleic acids, proteins, and cells, etc., with high sensitivity and selectivity [21–26].

So far, several works have been reported regarding virus detection based on FET biosensors. Guo and coworkers fabricated an ITO-based thin-film transistor biosensor in detecting avian influenza virus H5N1 with a sensitivity of 0.8×10^{-10} g·mL^{-1} [27]. Lieber and coworkers constructed a silicon nanowire field-effect transistor to capture single influenza A virus with rapid identification [28]. Liu and coworkers reported a MRGO-FET device to detect rotavirus in real fecal samples [29]. These works indicate that FET biosensors are effective tools for virus detection. However, the detection of virus in serum samples is difficult due to many other confounding factors in the sera negatively impacting sensitivity. On the other hand, the identification of EBOV is still challenging, such a filovirus as EBOV has yet been detected by FET biosensors.

Here, we present an effective way for directly electrical detecting EBOV using semiconducting RGO configured FETs, as illustrated in Fig. 1. After EBOV-specific antibodies are immobilized onto the RGO-based FET chip surfaces, conductance change occurs upon binding of the charged EBOV to the antibody. However, negligible conductance change appears when other non-specific viruses are applied onto the FET sensor. This work, for the first time, investigates EBOV detection with the RGO-FET biosensor in a sensitive and direct manner. The FET biosensor shows potential applications as POC in clinical medicine with its advantages including sensitive detection, high specificity and low cost.

Experimental section

Materials

Sodium dodecyl sulfate (SDS) was purchased from Generay Biotech Co. Ltd. (Shanghai, China, http://www.generay.com.cn/). 98% hydrazine was purchased from Aladdin Co. Ltd. (Shanghai, China, http://www.aladdin-e.com/). Graphite powder (99.99995%, 325 mesh) was purchased from Alfa Aesar Co. Ltd. (Tianjin, China, https://www.alfa.com/zh-cn/). Cy5 NHS ester was purchased from Nanjing bioorth biotech Co. Ltd. (Nanjing, China, https://shop151509095.taobao.com/). 1-Pyrenebutanoic acid succinimidyl ester (PASE) was purchased from Sigma-Aldrich (Shanghai, China, https://www.sigmaaldrich.com/). Bull serum albumin (BSA) was purchased from Thalys Co. Ltd. (Wuhan, China, http://www.thalys.net.cn/index.html). Streptavidin (SA) and glutaraldehyde were purchased from Solarbio Science & Technology Co. Ltd. (Beijing, China, http://www.solarbio.bioon.com.cn/). Anti-EpCAM antibody and Anti-CD9 antibody were purchased from Abcam Co. Ltd. (Shanghai, China, https://www.abcam.cn/). Inactivated EBOV whole virion and equine-origin antibody against the EBOV glycoprotein were supplied by Wuhan Institute of Virology, China. Healthy human serum samples were supplied by the Wuhan No. 1 Hospital, China, which was approved by the Ethics Committee of Wuhan No. 1 Hospital. Ultrapure water was gained from a Millipore water purification system (18.2 MΩ·cm resistivity, Milli-Q Direct 8). All the chemicals used in this research were of analytical level. All other chemicals, only if specified as reagent grade, are used without further purification.

Fabrication of the RGO-modified FET

RGO homogeneous solution was prepared by chemical reduction method, which was mentioned in our previous work [21–25]. The diluted RGO (0.2 mg·mL^{-1}) suspension was drop-casted onto the sensing channel region of the FET chip, and thermally annealed at 80 °C in a vacuum oven for 2 h so as to remove all hydrazine and improve the touch between the RGO and the electrodes. In order to obtain few-layer RGO, the chip was sonicated with Piranha solution (7:3 *v/v* concd H_2SO_4/35% H_2O_2) for 5 s, the RGO-FET devices were used for next modification.

Immobilization of equine-origin antibody against the EBOV glycoprotein on the FET devices

A three-step procedure was used to covalently attach the equine-origin antibody against the EBOV glycoprotein onto the surface of the RGO-FET biosensor. First, 5 mM PASE, as a cross-linker molecule, in dimethyl-

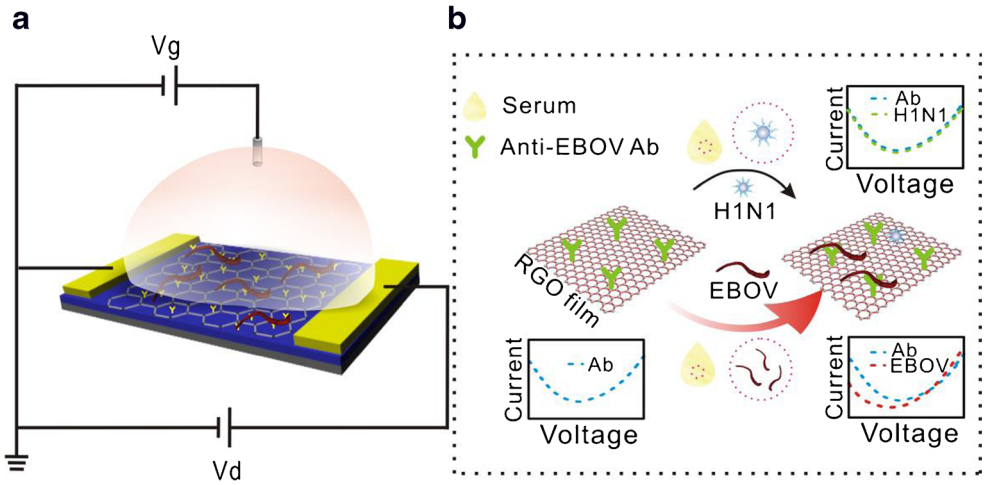

Fig. 1 Schematic presentation of the field effect transistor (FET) modified with reduced graphene oxide (RGO) for Ebola Virus (EBOV) detection

sulfoxide (DMSO) was dropped on the RGO channel. After incubation for 1 h, the chip was subsequently washed with pure DMSO, ethanol, and then DI water. Second, equine-origin antibody against the EBOV glycoprotein was immobilized on the chip surface for 2 h at room temperature. Third, the chip was subsequently passivated by reaction with BSA (1 $mg{\cdot}mL^{-1}$) for 1 h to avoid possible non-specific adsorption, rinsed by DI water and blown dry with N_2.

The detection of EBOV by the FET device

10 μL of EBOV in phosphate buffer saline (PBS) was dropped onto the equine-origin antibody modified channel and incubated for 30 min at 37 °C for immunoreactions. The chip was then rinsed with DI water to remove the unbound EBOV and dried with N_2. Finally, the chip was immersed with PBS for electrical measurement.

The detection of EBOV in serum

The EBOV in serum was prepared with different concentrations (12 $pg{\cdot}mL^{-1}$, 120 $pg{\cdot}mL^{-1}$, 1.2 $ng{\cdot}mL^{-1}$, 12 $ng{\cdot}mL^{-1}$) by spiking the EBOV in 10% normal human serum. Next, the prepared serum sample was dropped on the sensing surface where the equine-origin antibody was immobilized, allowing for incubation for 30 min at 37 °C. Then, the chip underwent necessary washing and subsequent electrical measurement as above-mentioned.

Electroanalytical measurements

Electrical measurements of the liquid-gate FET biosensor were performed at room temperature using a Keithley 4200 semiconductor characterization system coupled with a probe station (EverBeing BD-6, Taiwan). For electrical transfer characteristics curve measurements of the FET biosensor, the gate electrode was a silver wire reference electrode immersed in PBS with a constant bias of 0.1 V. Electrical output curves measurement was conducted at a designated V_g value.

Result and discussion

Characterizations

To characterize EBOV prior to the electrical measurement, transmission electron microscope (TEM, Hitachi, Japan) was performed. From the TEM image, it was clearly seen that the Ebola virus was a filamentous virus, about 900 nm in length and about 70 nm in diameter (Fig. 2a).

The RGO-FET biosensor was produced as previously described [21–25]. The anti-EBOV antibody was immobilized on the RGO surface by PASE. To verify the modification of anti-EBOV antibody on the RGO surface, the fluorescence characterization experiment was conducted. Anti-EBOV antibody was applied to the RGO surface before a silicon chip was treated with RGO and PASE. Subsequently, the chip was passivated by BSA, after which the fluorescent dye (Cy5) was applied to the antibody through the dehydration condensation reaction. The immobilization of the antibody was confirmed by fluorescence microscope. As shown in Fig. 2b, an obvious fluorescence was observed when anti-EBOV antibody was applied to the RGO surface. As a control in Fig. S1, no fluorescence was seen when only Cy5 was applied to the RGO surface, on which anti-EBOV antibody was not immobilized. The fluorescence experiments confirm that the anti-EBOV antibody has successfully been immobilized on the RGO surface.

Field emission scanning electron microscope (FE-SEM, CarlZeiss, Japan) was employed to characterize whether EBOV is conjugated to the immobilized

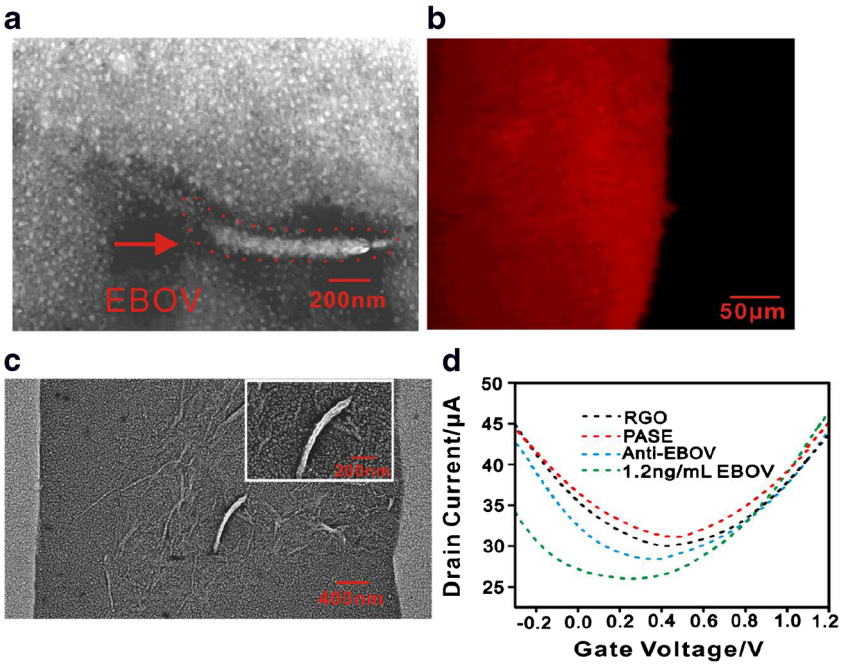

Fig. 2 **a** Transmission electron microscope (TEM) image of EBOV. **b** Fluorescence microscope image of the RGO-modified silicon chip observed after immobilization with anti-EBOV antibody and conjugation with Cy5 fluorescent dye. **c** Field emission scanning electron microscope (FE-SEM) image of EBOV inside the sensing channel. Inset: HR-FESEM image of the EBOV. **d** Plots of typical transfer curves at $V_d = 0.1$ V for the FET biosensor in the process of RGO formation, 1-Pyrenebutanoic acid succinimidyl ester (PASE) modification, anti-EBOV antibody immobilization, and EBOV binding

antibody. As mentioned previously, after the FET chip was immobilized with anti-EBOV antibody, EBOV was applied to the antibody-immobilized surface. As shown in Fig. 2c, filamentous viruses were observed inside the sensing channel, indicating that the RGO-FET immobilized with monoclonal anti-EBOV antibody successfully captured EBOV from specimen as a result of the specific antigen-antibody reaction. Also, the morphology of EBOV in FE-SEM is consistent with that of TEM.

In order to show that the progressive functionalization process was as successful as expected, the RGO-FET transfer characteristics curve in each step was confirmed. Figure 2d shows the typical transfer characteristics curve of the RGO-FET biosensor with an obvious ambipolar characteristic. The Dirac voltage of the pristine RGO-FET was found to be 0.420 V. After coupling of PASE to RGO, the Dirac voltage shifted to 0.461 V, suggesting that PASE introduced strong p-doping in RGO [30]. After binding of the anti-EBOV antibody, Dirac voltage was decreased by 0.095 V to a value of 0.325 V, which is contrasted to that of the pristine RGO-FET biosensor. The results further show that the anti-EBOV antibody has been immobilized on the PASE-RGO surface.

The zeta potential analysis of the EBOV in Fig. S2 shows that it is negatively charged, with a charge nearly of −26.7 mV. As discussed in our published literatures, the RGO-FET device is p-type doping. When EBOV (1.2 ng·mL^{-1}) was trapped on the chip, net carrier density increased, resulting in n-doping of the RGO-FET. This caused a left shift of the Dirac voltage from 0.325 V to 0.2 V in transfer curves as shown in Fig. 2d.

Reproducibility, stability, and reversibility

Firstly, in order to study the reproducibility of the RGO-FET biosensor, the transfer characteristics curves of 24 biosensors were recorded. As shown in the Fig. S3a, all 24 sensors had very similar current-gate voltage characteristics. The Dirac voltage of all biosensors was very close to a narrow range of about 0.425 ± 0.01 V (Fig. S3b), indicating that the biosensor achieved good reproducibility during the production process.

Secondly, the stability of the RGO-FET biosensor was explored by storing the anti-EBOV antibody functionalized device in a vacuum oven for several days. As shown in Fig. S3c, d, it can be seen that the Dirac voltage was slightly changed after the chip was stored at room temperature for 15 days. After 7 days and 15 days, the Dirac voltage retained more than 93.62 and 86.45% of its original value, respectively. The shift was likely caused by the nonspecific surface adsorption by air and water in the environment. The result means that the constructed biosensor has satisfactory stability.

Thirdly, reversibility experiments were performed by employing the anti-EBOV immobilized FET biosensor for EBOV detection over 3 cycles. After high ionic solution (NaCl, 1 M) was incubated with the chip for 5 min to dissociate the combination of EBOV and antibody, EBOV (12 ng·mL^{-1}) was applied again to the anti-EBOV immobilized FET biosensor to achieve reversibility [22, 31]. The transfer characteristic curves were measured repeatedly in 3 cycles. The shift of Dirac voltage was observed between 90 and 120 mV during 3 cycles of association and dissociation, indicating that the FET biosensor had the capability of reversibility. These potential oscillations of Dirac voltage were caused by 3 cycles,

as shown in Fig. S4. The results indicate that the anti-EBOV immobilized FET biosensor is reversible.

Specificity of the biosensor

Specificity is the ability to distinguish specific virus and other viruses, which is essential for practical medical and biological applications. To investigate the specificity of the biosensor towards EBOV, other viruses, such as H1N1, H3N2, H9N2, were used as negative control samples. Avian influenza virus (H1N1, H3N2, H9N2) can also cause fever symptoms similar to EBOV [32]. Therefore, they were selected as negative control (the concentration of 1 μg·mL^{-1}). Figure 3a reflects the response of the anti-EBOV antibody-modified RGO-FET biosensor to 3 different viruses. It's a negligible response when high concentrations of non-target viruses were applied to the FET biosensor. The negligible signal changes were caused probably by the nonspecific binding. In contrast, when the biosensor was interacted with a lower concentration of EBOV, an obvious left shift of Dirac voltage appeared in Fig. 3a (blue dashed line). As demonstrated in Fig. 3b, the changes of Dirac voltage shift in EBOV (1.2 ng·mL^{-1}) sample were significantly higher than those in negative controls. The Dirac voltage changes of H1N1, H3N2, H9N2, EBOV were about 12 mV, 8 mV, 11 mV and 87 mV, respectively. Therefore, it can be concluded that the RGO-FET biosensors showed a significant conductance change for EBOV, but the conductance change of other viruses is negligible. The results show that the prepared biosensor has high specificity to specific targets.

At the same time, different antibodies were also chosen to replace the EBOV-specific antibody to verify the specificity between anti-EBOV antibody and EBOV. As mentioned above, the chosen antibodies were immobilized on the RGO-FET biosensor to capture the EBOV. Anti-EpCAM antibody (EpCAM), anti-CD9 antibody (CD9), and streptavidin (SA) were selected as non-specific antibodies. As shown in Fig. 3c, after 1.2 ng·mL^{-1} of EBOV was incubated with nonspecific antibodies modified FET biosensor, slight changes of Dirac voltage appeared (dash line). However, when EBOV was incubated with its specific antibody, an obvious Dirac voltage change occurred as can be seen in Fig. 2d. Figure 3d summarizes the shift of Dirac voltage caused by 3 different antibodies immobilized FET biosensor interacted with EBOV. The Dirac voltage changes of the FET biosensor immobilized with nonspecific antibodies were 14 mV, 13 mV, 10 mV, respectively, whereas Dirac voltage change of the FET biosensor immobilized with equine-origin antibody against the EBOV glycoprotein was 125 mV. These results indicate that the RGO-FET biosensor was of high specificity.

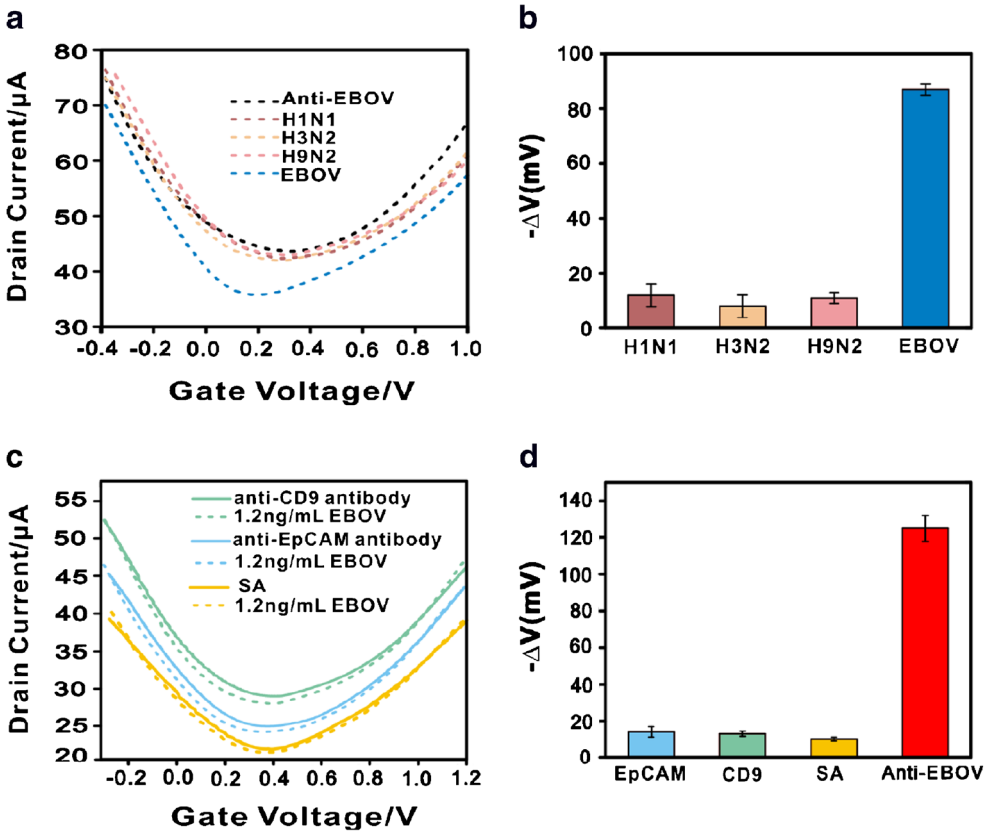

Fig. 3 **a** Transfer characteristics curves of the anti-EBOV antibody functionalized RGO-FET biosensor incubated with 1 μg·mL^{-1} H1N1, 1 μg·mL^{-1} H3N2, 1 μg·mL^{-1} H9N2, and 1.2 ng·mL^{-1} EBOV, respectively. **b** Summary of Dirac voltage shift of the RGO-FET biosensor: 1 μg·mL^{-1} H1N1, 1 μg·mL^{-1} H3N2, 1 μg·mL^{-1} H9N2, and 1.2 ng·mL^{-1} EBOV. **c** Transfer characteristics curves of the RGO-FET biosensor immobilized with 3 different antibodies: anti-EpCAM antibody (EpCAM) (blue solid line), or anti-CD9 antibody (CD9) (green solid line), or streptavidin (SA) (yellow solid line) to capture the EBOV. **d** Histograms of Dirac voltage change caused by the RGO-FET biosensors immobilized with 3 different antibodies and anti-EBOV antibody to capture EBOV (1.2 ng·mL^{-1}). Error bars correspond to standard deviation ($n = 3$)

Sensitivity of the biosensor

The sensitivity of the RGO-FET biosensor was evaluated by applying the EBOV at a concentration of 1.2 pg·mL^{-1}-12 μg·mL^{-1} to the antibody-immobilized RGO-FET biosensor. As shown in Fig. 4a, the Dirac voltage of the transfer characteristics curves gradually shifted to the left along with the increased concentrations from 2.4 to 120 ng·mL^{-1}. As mentioned above, the EBOV is negatively charged in PBS, resulting in n-doping of the RGO-FET after the EBOV was bound to the chip. Moreover, the change of Dirac voltage increased along with an increase in concentration. The sensor response to EBOV was quantified using the normalized Dirac voltage changes ($\Delta V/V_0 = (V\text{-}V_0)/V_0$), where V_0 is the initial Dirac voltage and V is the stabilized Dirac voltage after changing the concentration of EBOV. Figure 4b indicates the $\Delta V/V_0$% versus different concentrations of EBOV, which clearly shows that the left shift of Dirac point occurred along with the increase of EBOV concentrations. The method is semi-quantitative, and the detection range of EBOV in PBS is from 2.4×10^{-12} g·mL^{-1} to 1.2×10^{-7} g·mL^{-1}. The relevant calibration curve is $|\Delta V|/V_0(\%) = 6.9\text{lgC} + 9.87215$ (the logarithmic value of EBOV concentration is defined as lgC). The dashed line in Fig. 4b denotes the triple noise level from the blank control test. The limit of detection (LOD) of 2.4 pg·mL^{-1} was gained based on the signal/noise ratio ≥ 3.

In order to further explore the performance of the biosensor in practical sample detection, the different concentrations of EBOV spiked in human serum sample were also applied to the antibody-functionalized FET biosensor. As shown in Fig. S5a, the Dirac voltage of the transfer characteristics curves gradually shifted to the left along with the increased concentrations from 12 pg·mL^{-1} to 12 ng·mL^{-1}, which is similar with the above-mentioned results in Fig. 4a. Fig. S5b indicates the $\Delta V/V_0$% versus different concentrations of EBOV, clearly showing that the left shift of Dirac voltage occurred while EBOV concentrations were increased. The relevant calibration curve is $|\Delta V|/V_0(\%) = 5.7\text{lgC} + 12.04867$. (The logarithmic value of EBOV concentration defined as lgC). The dashed line in Fig. S5b denotes the triple noise level from the blank control test. The limit of detection (LOD) of 12 pg·mL^{-1} was gained based on the signal/noise ratio ≥ 3.

Furthermore, spike recovery test was performed to verify the applicability of the biosensor for detecting EBOV in physiological environment. As listed in

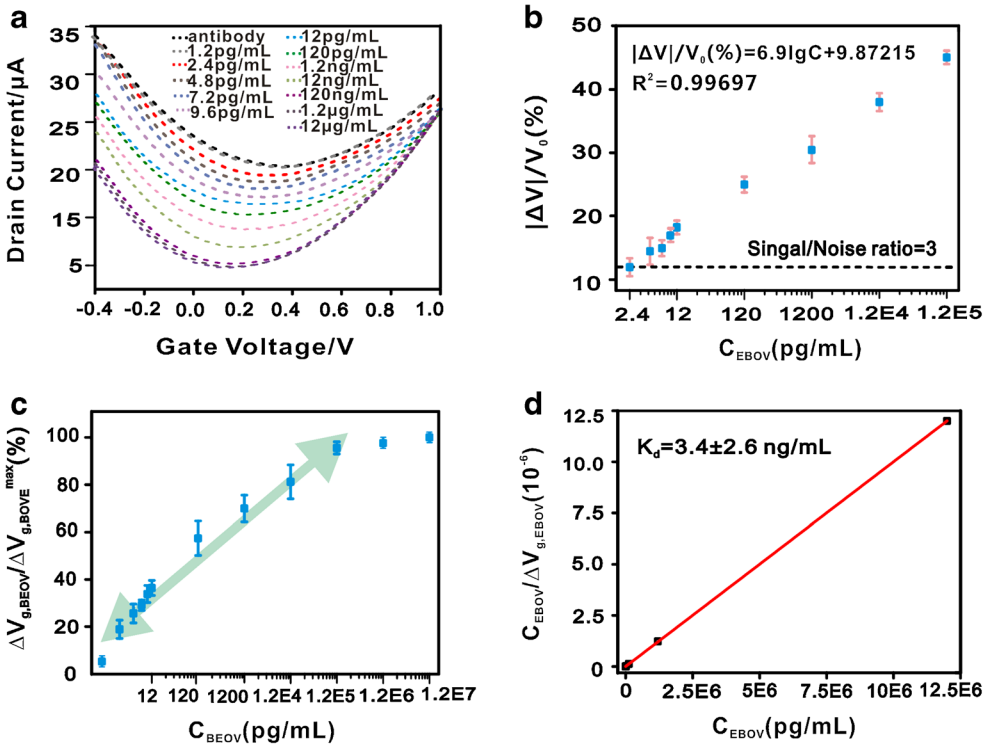

Fig. 4 **a** Transfer characteristics curves of the anti-EBOV antibody functionalized RGO-FET device to detect the EBOV at a series of concentrations (1.2 pg·mL^{-1}, 2.4 pg·mL^{-1}, 4.8 pg·mL^{-1}, 7.2 pg·mL^{-1}, 9.6 pg·mL^{-1}, 12 pg·mL^{-1}, 120 pg·mL^{-1}, 1.2 ng·mL^{-1}, 12 ng·mL^{-1}, and 120 ng·mL^{-1}, 1.2 μg·mL^{-1}, 12 μg·mL^{-1}). **b** The working curve of the RGO-FET biosensors for detection of EBOV at a series of concentrations (2.4 pg·mL^{-1}, 4.8 pg·mL^{-1}, 7.2 pg·mL^{-1}, 9.6 pg·mL^{-1}, 12 pg·mL^{-1}, 120 pg·mL^{-1}, 1.2 ng·mL^{-1}, 12 ng·mL^{-1}, and 120 ng·mL^{-1}). Dashed line represents the triple noise level from the blank control test. Error bars correspond to standard deviation ($n = 3$). **c** Normalized plot of $\Delta Vg_{,EBOV}/\Delta Vg_{,EBOV}{}^{max}$ (where $\Delta Vg_{,EBOV}{}^{max}$ is the saturated $\Delta Vg_{,EBOV}$) as a function of C_{EBOV} is summarized from the data in (Fig. 4a). **d** The least-squares fit to the Langmuir adsorption isotherm model, yielding $K_d = 3.4 \pm 2.6$ ng·mL^{-1} for the anti-EBOV antibody-EBOV complex

Table S1, the recovery for EBOV was from 93 to 105.6%, and the RSDs were between 4.9 and 6.3%. These results indicate that the biosensor has potential applications for detection of virus in clinical sample.

We next determined the binding affinity of anti-EBOV antibody to EBOV. The data from Fig. 4a were converted to the calibrated response $\Delta Vg,_{EBOV}/\Delta Vg._{EBOV}{}^{max}$ (where $\Delta Vg,_{EBOV}{}^{max}$ is the saturated $\Delta Vg,_{EBOV}$) as a function of C_{EBOV} in Fig. 4c. As displayed in Fig. 4c, it can be seen that the linear working range of the RGO-FET biosensor for EBOV detection spanned from 2.4×10^{-12} g·mL^{-1} to 1.2×10^{-7} g·mL^{-1} and then gradually became saturated about 1.2×10^{-6} g·mL^{-1}. Figure 4d plots the $C_{EBOV}/\Delta Vg,_{EBOV}$ against various EBOV concentrations (C_{EBOV}), and the dissociation constant (K_d) of the anti-EBOV antibody-EBOV complex was calculated to be 3.4 ± 2.6 ng·mL^{-1}, which was determined from the least-squares fit to the Langmuir adsorption isotherm model.(Eqs. 1, 2) [33].

$$\frac{C_{EBOV}}{\Delta V_{gEBOV}} = \frac{C_{EBOV}}{\Delta V^{max}_{gEBOV}} + \frac{1}{\Delta V^{max}_{g,EBOV}} kd \quad (1)$$

$$\Delta V_{g,EBOV}(\%) = \frac{\Delta V_{g,EBOV} - \Delta V^{0}_{g}EBOV}{\Delta V^{max}_{gEBOV} - \Delta V^{0}_{g}EBOV} \times 100(\%) \quad (2)$$

where the $\Delta Vg,_{EBOV}{}^{0}$ is the calibrated response at $C_{EBOV} = 0$ that induces no detectable signal, and $\Delta Vg,_{EBOV}{}^{max}$ is the saturated calibrated response at high C_{EBOV}.

The immunosensors of RGO-FET have been intensively investigated. Hao and coworkers studied a real-time monitoring of insulin using a RGO-FET nanosensor, in which $K_d = 203$ ng·mL^{-1} [30]. Our result ($K_d = 3.4 \pm 2.6$ ng·mL^{-1}) is lower than the reported results, indicating that there is a high binding affinity between anti-EBOV antibody and EBOV. The dissociation constant generally reported for anti-EBOV antibody against EBOV ranged from 2 to 20 nM [34]. Thus, the RGO-FET biosensor shows sufficiently high binding affinity, making it ideal as a sensitive tool for practical EBOV detection in clinical diagnosis.

A couple of technologies, such as electroluminescent, fluorescence counting strategies, have been used for inactive EBOV detection. Compared with other works, an overview on recently reported determination of EBOV is summarized in Table S2. For instance, Wu and coworkers revealed a method for EBOV detection based on electroluminescent nanospheres coupled with immunomagnetic separation with a sensitivity of 5.2 pg·mL^{-1} [13]. To further challenge high sensitivity, Hong and coworkers established a cellular beacons-mediated counting to detect EBOV on an integrated micromagnetic platform, in which a high sensitivity of 2.6 pg·mL^{-1} was achieved [15]. Albeit these methods enable highly sensitive and precise detection of EBOV directly, they frequently fail to satisfy many other desirable features such as cost-efficiency.

Detection of the EBOV in clinical samples

To survey the applicability of this RGO-FET in clinical sample, the RGO-FET biosensor was used for detecting EBOV in serum samples. The inactivated EBOV (12 ng·mL^{-1}) was spiked to different concentrations of 10%, 30%, 50%, 70%, 100% normal human serum. In the experiment, EBOV (12 ng·mL^{-1}) in different concentrations of serum for EBOV detection were chosen for positive control, while the different concentrations of serum without target EBOV was used as blank control. In the absence of EBOV, a slight shift of Dirac voltage was observed (negative, Fig. 5), as serum is complex and can cause slight voltage changes due to non-specific adsorption. On the contrary, the remarkable shift of Dirac voltage was observed in the presence of EBOV. Simultaneously, the EBOV can be detected with the increase of serum concentration, and even in whole serum. To make the comparison clearer, the shift of Dirac point for EBOV detection in 10%, 30%, 50%, 70%, 100% serum was about 92 mV, 87 mV, 71 mV, 56 mV, 51 mV, respectively. Therefore, it is proved that the RGO-FET biosensor has a potential application prospect in detecting EBOV in real clinical samples.

Conclusion

We have established a highly sensitive RGO-FET biosensor for EBOV detection in serum. We have shown that direct detection of EBOV can be realized by immobilizing equine-origin antibody against the EBOV glycoprotein on the RGO FET chip surface, and that high binding affinity between EBOV and the corresponding antibody can be attained. This

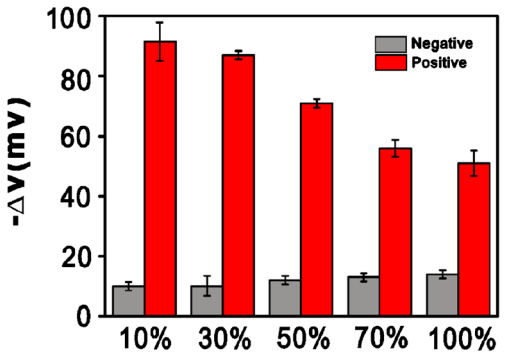

Fig. 5 Histogram of Dirac voltage change of the RGO-FET biosensor capturing inactivated EBOV in different concentrations of 10%, 30%, 50%, 70%, 100% normal human serum. Positive (with 12 ng·mL^{-1} EBOV). Negative (without EBOV). Error bars represent standard deviations of measurements ($n = 3$)

sensing platform is also attractive from the standpoint of high sensitivity and specificity achieved. In addition, the FET biosensor can directly detect the EBOV in whole serum, making it possible for practical applications. Nevertheless, the major limitations of the method lie in the following aspects: 1) The chip-to-chip variation exists because the fabrication of each RGO-FET sensor is variable; 2) The real sample detection is still challenging because the blood is consisted of red cells, white cells, etc., and these elements can affect the detection; 3) The surface density of antibody and the binding efficiency between antibody and virus are tough to control due to inherent issues like steric hindrance and orientation. Even though, we believe that the sensing strategy can cost-effectively detect EVD and potentially reduce the spread of EVD and patient death. This method has great application potential as POCT tools in remote areas.

Acknowledgements This work was supported by the National Natural Science Foundation of China (Nos. 21475034, 21675041, and 61390504).

Compliance with ethical standards The author(s) declare that they have no competing interests. All procedures performed in studies involving human participants were in accordance with the ethical standards of the institutional and/or national research committee and with the 1964 Helsinki declaration and its later amendments or comparable ethical standards.

References

1. Mahanty S, Bray M (2004) Pathogenesis of filoviral haemorrhagic fevers. Lancet Infect Dis 4:487–498
2. Feldmann H, Geisbert TW (2011) Ebola haemorrhagic fever. Lancet 377:849–862
3. Takada AJU (2011) Filoviruses. Uirusu 62:197–208
4. Nkoghe D, Leroy EM, Toung-Mve M, Gonzalez JP (2012) Cutaneous manifestations of filovirus infections. Int J Dermatol 51:1037–1043
5. Kiley MP, Bowen ETW, Eddy GA, Isaäcson M, Johnson KM, Mccormick JB, Murphy FA, Pattyn SR, Peters D, Prozesky OW (1982) Filoviridae: a taxonomic home for Marburg and Ebola viruses? Intervirology 18:24–32
6. Niikura M, Ikegami T, Saijo M, Kurane I, Miranda ME, Morikawa S (2001) Detection of ebola viral antigen by enzyme-linked immunosorbent assay using a novel monoclonal antibody to nucleoprotein. J Clin Microbiol 39:3267–3271
7. Krähling V, Becker D, Rohde C, Eickmann M, Eroğlu Y, Herwig A, Kerber R, Kowalski K, Vergaraalert J, Becker S (2016) Development of an antibody capture ELISA using inactivated Ebola Zaire Makona virus. Med Microbiol Immunol 205:173–183
8. Ikegami T, Saijo M, Niikura M, Miranda ME, Calaor AB, Hernandez M, Manalo DL, Kurane I, Yoshikawa Y, Morikawa S (2013) Development of an immunofluorescence method for the detection of antibodies to Ebola virus subtype Reston by the use of recombinant nucleoprotein-expressing HeLa cells. Microbiol Immunol 46:633–638
9. Drosten C, Gottig S, Schilling S, Asper M, Panning M, Schmitz H, Gunther S (2002) Rapid detection and quantification of RNA of ebola and Marburg viruses, Lassa virus, Crimean-Congo hemorrhagic fever virus, rift valley fever virus, dengue virus, and yellow fever virus by real-time reverse transcription-PCR. J Clin Microbiol 40:2323–2330
10. Kuhn JH, Dodd LE, Wahl-Jensen V, Radoshitzky SR, Bavari S, Jahrling PB (2011) Evaluation of perceived threat differences posed by filovirus variants. Biosecur Bioterror 9:361–371
11. Semper AE, Broadhurst MJ, Richards J, Foster GM, Simpson AJ, Logue CH, Kelly JD, Miller A, Brooks TJ, Murray M, Pollock NR (2016) Performance of the genexpert ebola assay for diagnosis of ebola virus disease in Sierra Leone: a field evaluation study. PLoS Med 13:e1001980
12. van Griensven J, Edwards T, de Lamballerie X, Semple MG, Gallian P, Baize S, Horby PW, Raoul H, Magassouba N, Antierens A, Lomas C, Faye O, Sall AA, Fransen K, Buyze J, Ravinetto R, Tiberghien P, Claeys Y, De Crop M, Lynen L, Bah EI, Smith PG, Delamou A, De Weggheleire A, Haba N (2016) Evaluation of convalescent plasma for ebola virus disease in Guinea. N Engl J Med 374:33–42
13. Wu Z, Hu J, Zeng T, Zhang ZL, Chen J, Wong G, Qiu X, Liu W, Gao GF, Bi Y, Pang DW (2017) Ultrasensitive ebola virus detection based on electroluminescent nanospheres and immunomagnetic separation. Anal Chem 89:2039–2048
14. Tsang M-K, Ye W, Wang G, Li J, Yang M, Hao J (2016) Ultrasensitive detection of ebola virus oligonucleotide based on upconversion nanoprobe/nanoporous membrane system. ACS Nano 10:598–605
15. Hong SL, Zhang YN, Liu YH, Tang M, Pang DW, Wong G, Chen J, Qiu X, Gao GF, Liu W, Bi Y, Zhang ZL (2018) Cellular-beacon-mediated counting for the ultrasensitive detection of ebola virus on an integrated micromagnetic platform. Anal Chem 90:7310–7317
16. Duan X, Lieber CM (2015) Nanoscience and the nano-bioelectronics frontier. Nano Res 8:1–22
17. Song S, Qin Y, He Y, Huang Q, Fan C, Chen HY (2010) Functional nanoprobes for ultrasensitive detection of biomolecules. Chem Soc Rev 39:4234–4243
18. Zhang A, Lieber CM (2016) Nano-bioelectronics. Chem Rev 116: 215–257
19. Li J, Zhang Y, To S, You L, Sun Y (2011) Effect of nanowire number, diameter, and doping density on nano-FET biosensor sensitivity. ACS Nano 5:6661–6668
20. Zhang GJ, Zhang G, Chua JH, Chee RE, Wong EH, Agarwal A, Buddharaju KD, Singh N, Gao Z, Balasubramanian N (2008) DNA sensing by silicon nanowire: charge layer distance dependence. Nano Lett 8:1066–1070
21. Cai B, Huang L, Zhang H, Sun Z, Zhang Z, Zhang GJ (2015) Gold nanoparticles-decorated graphene field-effect transistor biosensor for femtomolar microRNA detection. Biosens Bioelectron 74: 329–334
22. Lei YM, Xiao MM, Li YT, Xu L, Zhang H, Zhang ZY, Zhang GJ (2017) Detection of heart failure-related biomarker in whole blood with graphene field effect transistor biosensor. Biosens Bioelectron 91:1–7
23. Xie H, Li YT, Lei YM, Liu YL, Xiao MM, Gao C, Pang DW, Huang WH, Zhang ZY, Zhang GJ (2016) Real-time monitoring of nitric oxide at single-cell level with porphyrin-functionalized graphene field-effect transistor biosensor. Anal Chem 88:11115–11122
24. Zhang C, Xu JQ, Li YT, Huang L, Pang DW, Ning Y, Huang WH, Zhang Z, Zhang GJ (2016) Photocatalysis-induced renewable field-effect transistor for protein detection. Anal Chem 88:4048–4054
25. Cai B, Wang S, Huang L, Ning Y, Zhang Z, Zhang GJ (2014) Ultrasensitive label-free detection of PNA-DNA hybridization by

reduced graphene oxide field-effect transistor biosensor. ACS Nano 8:2632–2638
26. Zheng C, Huang L, Zhang H, Sun Z, Zhang Z, Zhang GJ (2015) Fabrication of ultrasensitive field-effect transistor DNA biosensors by a directional transfer technique based on CVD-grown graphene. ACS Appl Mater Interfaces 7:16953–16959
27. Guo D, Zhuo M, Zhang X, Xu C, Jiang J, Gao F, Wan Q, Li Q, Wang T (2013) Indium-tin-oxide thin film transistor biosensors for label-free detection of avian influenza virus H5N1. Anal Chim Acta 773:83–88
28. Patolsky F, Zheng G, Hayden O, Lakadamyali M, Zhuang X, Lieber CM (2004) Electrical detection of single viruses. PNAS 101:14017–14022
29. Liu F, Kim YH, Cheon DS, Seo TS (2013) Micropatterned reduced graphene oxide based field-effect transistor for real-time virus detection. Sensors Actuators B Chem 186:252–257
30. Hao Z, Zhu Y, Wang X, Rotti PG, DiMarco C, Tyler SR, Zhao X, Engelhardt JF, Hone J, Lin Q (2017) Real-time monitoring of insulin using a graphene field-effect transistor aptameric nanosensor. ACS Appl Mater Interfaces 9:27504–27511
31. Duan XX, Li Y, Rajan NK, Routenberg DA, Modis Y, Reed MA (2012) Quantification of the affinities and kinetics of protein interactions using silicon nanowire biosensors. Nat Nanotechnol 7:401–407
32. Beeching NJ, Fenech M, Houlihan CF (2014) Ebola virus disease. BMJ 349:g7348
33. Li BR, Hsieh YJ, Chen YX, Chung YT, Pan CY, Chen YT (2013) An ultrasensitive nanowire-transistor biosensor for detecting dopamine release from living PC12 cells under hypoxic stimulation. J Am Chem Soc 135:16034–16037
34. Liu JL, Shriver-Lake LC, Anderson GP, Zabetakis D, Goldman ER (2017) Selection, characterization, and thermal stabilization of llama single domain antibodies towards ebola virus glycoprotein. Microb Cell Factories 16:223